

# Relativistic Jet Stability and Structure from the Alfvén Point Outwards

Philip E. Hardee<sup>1</sup>, Alexander Rosen<sup>1</sup>, Philip A. Hughes<sup>2</sup> and G. Comer Duncan<sup>3</sup>

(1) *University of Alabama  
Department of Physics & Astronomy, Tuscaloosa, AL 35487 USA*

(2) *University of Michigan  
Astronomy Department, Ann Arbor, MI 48109 USA*

(3) *Bowling Green State University  
Department of Physics & Astronomy, Bowling Green, OH 43403 USA*

## Abstract.

The amplitude of jet distortions and accompanying pressure and velocity fluctuations resulting from Kelvin-Helmholtz instability of three dimensional relativistic jets are explored. The effect of instability on jets as they accelerate from sub- to super-Alfvénic speeds is explored and a relativistic stabilization mechanism for trans-Alfvénic jets is proposed. The level to which asymmetric instabilities on supermagnetosonic relativistic jets will grow is predicted theoretically and a Doppler boosted “apparent” emissivity is computed. Effects due to helically twisted filamentary structure produced by asymmetric modes of instability should be readily observable on relativistic jets.

## 1. Introduction

There is compelling evidence for relativistic highly collimated jets in both galactic [1] and extragalactic objects [2]. In the galactic “superluminals” GRS 1915+105 [3] and GRO J1655-40 [4] [5] the observed proper motions indicate jet flow speeds on the order of 92% of light speed. Among the extragalactic superluminals, observed motions indicate jet flow speeds as large as 99.9% of light speed, e.g., 3C 345 [6]. It is quite likely that all jets produced by black holes in binary star systems [7] or in AGN’s [8] [9] are initially relativistic.

Recent jet acceleration and collimation schemes require dynamically strong magnetic fields close to the central engine. Numerical studies [10] [11] [12] [13] show that the jets created in this fashion pass through slow magnetosonic, Alfvénic, and fast magnetosonic critical points. The ultimate jet velocity may depend on the configuration of the magnetic field [14], and the jets accelerate up to asymptotic speeds that may be only a few times the Alfvén speed at the Alfvén point – at the Alfvén point the jet speed equals the Alfvén speed [15]. This basic acceleration and collimation process may be the same for all classes of objects that emit jets [16].

Jets are susceptible to the Kelvin-Helmholtz instability. The K-H instability of three-dimensional (3D) jets with purely poloidal or purely toroidal magnetic fields

[17] [18] [19] [20], and of jets containing force-free helical magnetic fields [21] [22] has been extensively investigated in the supermagnetosonic limit. This instability can lead to the development of highly organized helical structures and ultimately to disruption of highly collimated flow as mass is entrained into the jet from the external environment [23]. In general, spatial or temporal growth rates associated with the K-H instability are found to increase as the magnetosonic Mach number decreases provided the jet is super-Alfvénic. Unlike purely fluid flows which are unstable when subsonic, the poloidally magnetized jet is predicted to be nearly completely stabilized to the K-H instability when the jet is sub-Alfvénic [24]. Here in § 2 and § 3 we consider the types of organized structure and stability properties that exist on supermagnetosonic and trans-Alfvénic non-relativistic jets, respectively. In § 4 and § 5 we consider the stabilizing effects of relativistic jet speeds in the trans-Alfvénic and supermagnetosonic regimes.

## 2. The Supermagnetosonic Non-Relativistic Jet

Structures that arise on jets can be considered to consist of Fourier components of the form

$$f_1(r, \phi, z) = f_1(r) \exp[i(kz \pm n\phi - \omega t)]$$

where flow is along the  $z$ -axis, and  $r$  is in the radial direction with the flow bounded by  $r = R$ .  $k$  is the longitudinal wavenumber,  $n$  is an integer azimuthal wavenumber, for  $n > 0$  the wavefronts are at an angle to the flow direction, the angle of the wavevector relative to the flow direction is  $\theta = \tan(n/kR)$ , and  $\pm n$  refers to wave propagation in the clockwise and counterclockwise directions around the jet circumference.  $n = 0, 1, 2, 3, 4$ , etc. correspond to pinch, helical, elliptical, triangular, rectangular, etc. “normal” mode distortions of the jet, respectively. For a jet with uniform density, temperature and axial magnetic field (top hat profile) and a uniform external medium, the propagation and growth or damping of the Fourier components is described by a dispersion relation [25]. When the flow is supermagnetosonic, each normal mode,  $n$ , contains a growing single “surface” wave and multiple “body” wave solutions that satisfy the dispersion relation (cf., Figure 2). The growth rate of normal mode surface and body waves has a maximum that is inversely proportional to the magnetosonic Mach number at a wavelength that is approximately proportional to the magnetosonic Mach number. The body wave modes exist only for wavelengths less than some maximum wavelength.

Figure 1 shows the maximum displacements associated with asymmetric surface wave modes at the fastest growing wavelength and of symmetric and asymmetric body wave modes at the maximum unstable wavelength [26] [27]. The body modes show a reversal in fluid displacement at “null” surfaces interior to the jet surface. For example, the first pinch body mode has a null displacement surface (fluid does not move radially) at jet center. The second pinch body mode shows an additional null displacement surface between jet center and jet surface. The third pinch body mode shows two null displacement surfaces between jet center and jet surface. Pressure fronts inside the jet become more oblique to the jet axis as the body wave mode number increases. The radial displacement associated with an asymmetric “surface” wave mode  $n > 0$  is approximately given by  $\xi_{r,n}(r) \approx \xi_{r,n}^s(r/R)^{n-1}$  where  $\xi_{r,n}^s$  is the surface amplitude [28]. Inside the jet surface the displacement is rotated in azimuthal angle relative to displacement at the jet surface in addition to changes

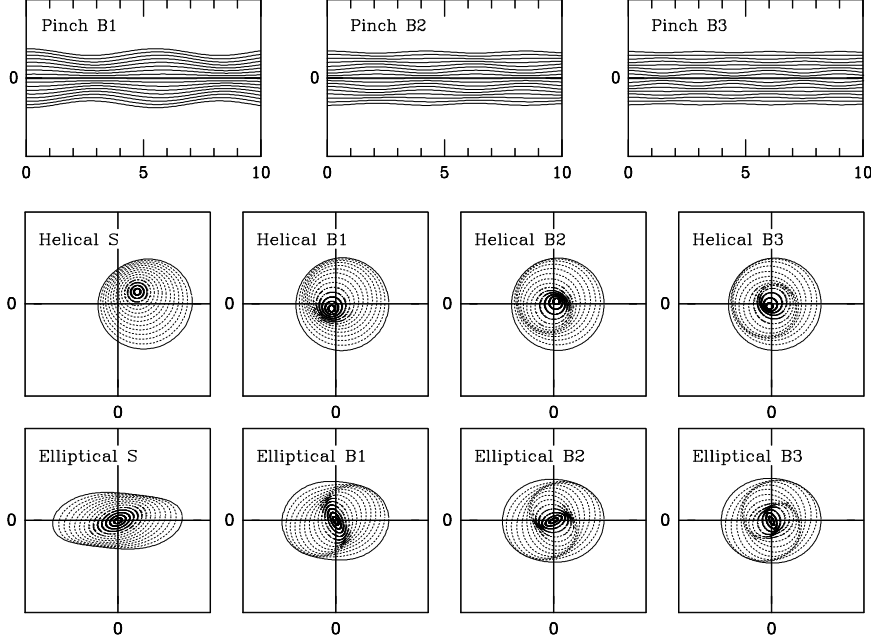


**Figure 1.** Axial cross sections associated with maximum pinch body mode (B1, B2, B3) displacements and transverse cross sections associated with maximum helical and elliptical surface (S) and body mode (B1, B2, B3) displacements.

in the displacement amplitude. Fluid displacements associated with the asymmetric body waves show a much larger azimuthal rotation and have larger amplitudes in the jet interior relative to the jet surface than for the surface wave [26]. Only the helical surface and body waves lead to jet displacement off the initial axis. Jet distortions comparable to the amplitudes shown in Figure 1 have been observed in non-relativistic 3D MHD numerical simulations [26].

### 3. The Trans-Alfvénic Non-Relativistic Jet

When a jet is sub-Alfvénic the helical and higher order ( $n > 0$ ) surface modes are stable, but rapidly destabilize when the jet becomes super-Alfvénic. The stability and behavior of the normal mode solutions can be investigated analytically in the limit  $\omega \rightarrow 0$ . In this limit the real part of the pinch mode ( $n = 0$ ) surface wave solution becomes [24]

$$\omega/k \approx u \pm \left\{ \frac{1}{2} \left( V_A^2 + \frac{V_A^2 a_j^2}{a_{ms}^2} \right) \pm \frac{1}{2} \left[ \left( V_A^2 + \frac{V_A^2 a_j^2}{a_{ms}^2} \right)^2 - 4 \frac{V_A^4 a_j^2}{a_{ms}^2} \right]^{1/2} \right\}^{1/2}.$$

In the equation above  $V_A = (B^2/4\pi\rho_j)^{1/2}$ ,  $a_j$  is the jet sound speed, and  $a_{ms} \equiv (a_j^2 + V_A^2)^{1/2}$  is the magnetosonic speed. The imaginary part of the solution is vanishingly small in the low frequency limit. These solutions are related to fast (+)

and slow (–) magnetosonic waves propagating with ( $u+$ ) and against ( $u-$ ) the jet flow speed  $u$ , but strongly modified by the jet-external medium interface. Numerical solution of the dispersion relation reveals that a growing solution is associated with the backwards moving (in the jet fluid reference frame) solution related to the slow magnetosonic wave and the pinch mode surface wave is unstable on sub-Alfvénic and super-Alfvénic jets.

When a jet is sub-Alfvénic the helical and higher order ( $n > 0$ ) surface modes are stable [20] [24] and have an outwards moving purely real solution given by

$$\omega/k \approx u + V_A .$$

On the super-Alfvénic jet in the limit  $\omega \rightarrow 0$  all higher order modes ( $n > 0$ ) have surface wave solutions given by

$$\omega/k \approx \frac{\eta}{1+\eta} u \left\{ 1 \pm i \frac{[1 - (1+\eta)V_A^2/u^2]^{1/2}}{\eta^{1/2}} \right\} .$$

where the jet to external medium density ratio  $\eta \equiv \rho_j/\rho_x$ . Wave growth corresponds to the plus sign. Note that in the dense jet limit, i.e.,  $\eta \rightarrow \infty$ , this expression reduces to  $\omega/k \approx u \pm V_A$ , and thus the surface waves are related to Alfvén waves propagating with and against the jet flow speed but strongly modified by the jet-external medium interface. The unstable growing solution is associated with the backwards moving (in the jet fluid reference frame) wave. The surface wave speed in the observer frame,  $(\omega/k)_{Real}$ , and the growth rate,  $(\omega/k)_{Imag}$ , are strongly dependent on the density ratio. Higher jet density is stabilizing.

Numerical simulations of low density 3D MHD jets [24] verify that “light” jets destabilize rapidly near to the Alfvén point. In the simulations, the observed rapid development of instability leads to rapid mass entrainment and slowing of the “light” jets in the trans-Alfvénic region before the jets can become supermagnetosonic.

#### 4. Trans-Alfvénic Relativistic Jet Stabilization

The rapid development of instability at the Alfvén point and subsequent mass entrainment and slowing of “light” jets can be overcome. To see what is required for enhanced stability of the helical and higher order normal modes we consider the asymmetric normal mode solutions to the fully relativistic MHD dispersion relation in the limit  $\omega \rightarrow 0$  [29]:

$$\omega/k \approx \frac{\gamma^2 \eta}{1 + \gamma^2 [1 + (V_A/\gamma c)^2] \eta} u \left\{ 1 \pm i \frac{[1 - (1+\eta)(V_A/\gamma u)^2 - (\eta/\gamma^2)(V_A/c)^4]^{1/2}}{\gamma \eta^{1/2}} \right\}$$

where  $\eta \equiv W_j/W_x$ ,  $V_A \equiv (B^2/4\pi W_j)^{1/2}$ ,  $\gamma$  is the Lorentz factor, and the enthalpy  $W \equiv \rho + (\frac{\Gamma}{\Gamma-1})(P/c^2)$  where  $\Gamma$  is the adiabatic index. A positive value for the imaginary part of the frequency indicates instability. Note that the Alfvén speed can be superluminal. When  $[1 - (1+\eta)(V_A/\gamma u)^2 - (\eta/\gamma^2)(V_A/c)^4] < 0$  the jet is stable to the asymmetric normal modes, and in the limit  $\eta \rightarrow \infty$  it can be shown that

$$\omega/k \approx \frac{u \pm v_w}{1 \pm (uv_w/c^2)} \quad \text{and} \quad v_w = \frac{V_A}{(1 + V_A^2/c^2)^{1/2}} .$$

Thus, helical and higher order surface waves are related to Alfvén waves and, of course, the Alfvén waves propagate at less than lightspeed. The unstable solution is associated with the backwards moving (in the jet fluid reference frame) wave. When unstable the wave speed in the observer frame,  $(\omega/k)_{Real} \approx [\gamma^2\eta/(1+\gamma^2\eta)]u$ , increases and the growth rate is reduced as  $\gamma\eta^{1/2}$  increases. Thus, relativistic jets are effectively heavier and can pass through the Alfvén point with less rapid development of instability. These effectively heavier jets should be much less susceptible to slowing by mass entrainment [23].

## 5. Supermagnetosonic Relativistic Jet Structure

### 5.1. Theory & Axisymmetric Numerical Simulation Compared

Jets that survive the trans-Alfvénic region without serious mass entrainment and slowing will become supermagnetosonic with continued expansion. The amplitude to which normal mode structures can develop on supermagnetosonic relativistic jets can be deduced from numerical simulations of relativistic jets [30] [27]. In the simulations the jets are perturbed by strong pressure waves driven into the jet at approximately constant spatial interval by large scale vortices in the surrounding cocoon. The cocoon vortices induce oblique pressure disturbances in the jet at approximately the relativistic Mach angle. This oblique disturbance is at the appropriate angle to couple to the third pinch body mode (B3 in Figure 1).

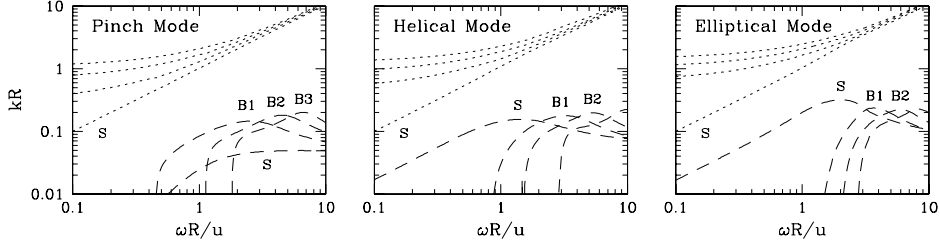
Figure 2 shows normal mode solutions to the dispersion relation appropriate to a relativistic jet simulation [30] (Lorentz factor  $\gamma = 5$ , Mach number  $\gamma M_j \approx 10.5$  where  $M_j \equiv u/a_j$ , and the jet resides in a hot tenuous cocoon where  $M_c \equiv u/a_c \approx 1.5$ ) for surface (S) and the first three body waves (B1, B2, B3) of the pinch, helical and elliptical normal modes. These solutions are typical of supermagnetosonic jet flows. With the exception of the surface pinch mode all wave modes have a maximum in the growth rate (dashed lines). The body wave modes have a longest unstable wavelength (determined from the real part of the wavenumber where the imaginary part goes to zero) which is slightly shorter than the longest allowed wavelength (determined from the wavenumber in the limit  $\omega \rightarrow 0$ ). Figure 2 also contains a comparison between pressure, axial, and transverse (radial) velocity fluctuations seen in the numerical simulation with theoretically derived oscillations associated with the B3 pinch body mode at the longest unstable wavelength. The comparison indicates that a maximum theoretical pressure fluctuation,  $2 > P/P_0 > 0$ , successfully reproduces the observed maximum transverse (radial) velocity oscillations seen in the numerical simulation far behind the jet front, i.e.,  $15 < z/R_0 < 20$ .

### 5.2. Predicted Asymmetric Relativistic Jet Structure

The maximum pressure fluctuation criterion ( $2 > P/P_0 > 0$ ) found from axisymmetric numerical simulations can be used to predict the cross section distortions and asymmetric structural features that will appear on 3D supermagnetosonic relativistic jets. In Figure 3 (top panels) we plot the maximum cross section distortions for the elliptical surface wave mode and first elliptical body wave mode at the maximum growth rate and longest unstable wavelength, respectively, where we have used the dispersion relation solutions appropriate to the relativistic jet shown in Figure 2, i.e.,  $u/c = 0.98$  and  $\gamma = 5.0$ . Comparison between these distortions and those allowed

## SuperMagnetosonic Relativistic Jet Stability

Normal mode analysis for  $u/c = 0.98$



## Maximum Pressure and Velocity Fluctuations

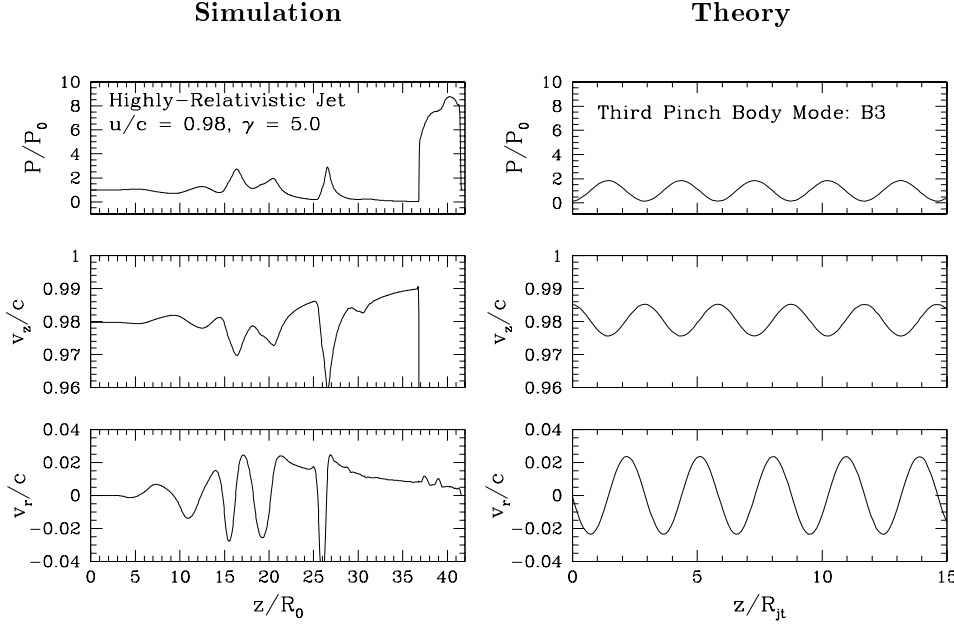
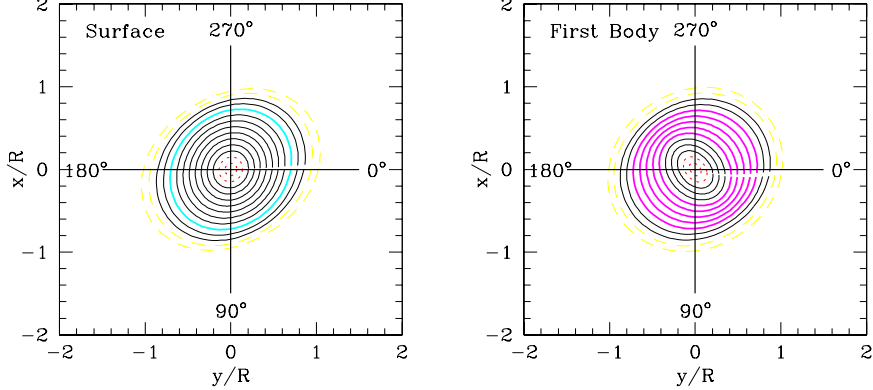


**Figure 2.** Solutions to the dispersion relation for the highly relativistic numerical simulation (top panels). The dotted (dashed) lines give the real (imaginary) part of the wavenumber as a function of the angular frequency. Pressure and velocity fluctuations seen in the numerical simulation just off the jet axis, and pressure and velocity fluctuations associated with the B3 pinch body mode just off the jet axis are shown in the bottom panels.

on non-relativistic jets (see Figure 1) shows a considerable reduction in the allowed distortion. In general, we have found that the allowed distortion decreases as the relativistic Mach number increases at wavelengths near to the maximum growth rate (surface wave) or between the longest unstable wavelength and the maximally growing wavelength (body waves). At longer wavelengths the surface wave elliptical distortion

### Maximum Relativistic Jet Elliptical Displacement



### Maximum Pressure Fluctuation & Apparent Emissivity

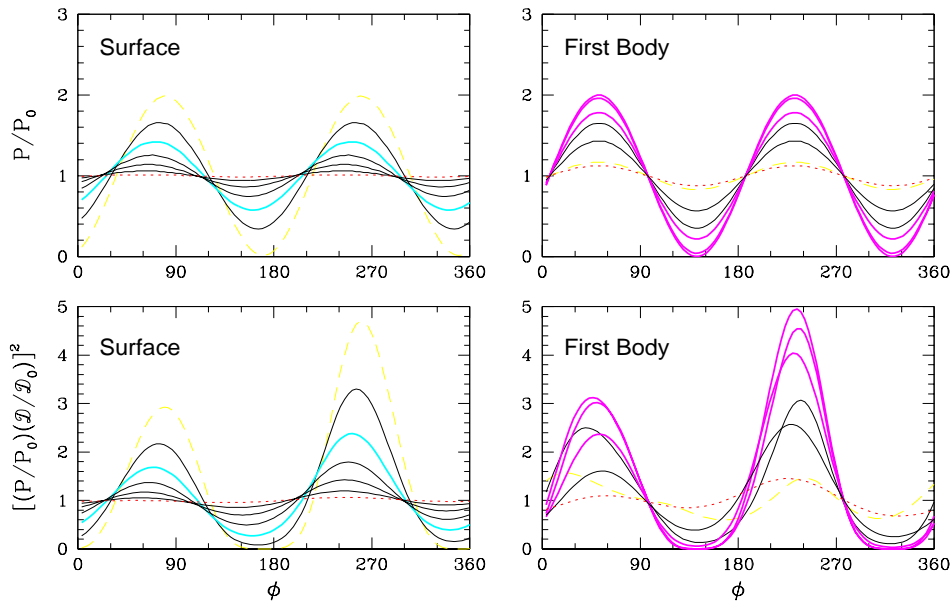


**Figure 3.** Maximum transverse cross section elliptical surface and first body wave distortions (top panels), and the accompanying pressures and “apparent” emissivities around the displacement contours (bottom panels). The dashed (heavy solid, dotted) lines in the cross sections correspond to the dashed (heavy solid, dotted) line(s) in the pressure and apparent emissivity plots.

to the cross section can be larger than that shown in Figure 3 [31].

High pressure regions accompanying the distortions along with the Doppler boosting factor

$$D \equiv \{\gamma[1 - (v/c)\cos\theta]\}^{-1}$$

and an angle  $\theta = 1/\gamma + \delta\theta$  where  $\delta\theta$  represents the perturbation to the initial flow angle,  $\theta = 1/\gamma$ , with respect to the line of sight, allows us to construct an “apparent” synchrotron emissivity  $P^2 D^2$ . For the elliptical distortions shown in Figure 3,  $|\delta\theta| < 0.1$  radian, and we also have found that  $|\delta\theta| \propto 1/\gamma$ . The curves of pressure and “apparent” emissivity shown in Figure 3 are taken around the displacement contours where the dashed (dotted) lines are at the jet surface (center), respectively, and the heavy lines indicate the innermost contour of the high pressure region (surface elliptical mode) or highest pressure region (first elliptical body mode). The pressure and apparent emissivity plots indicate that two bright filaments will accompany an elliptical distortion. These filaments will wind around the jet as the elliptical distortion rotates spatially down the jet and can show brightness asymmetry as a result of variation in the Doppler boosting factor induced by a varying flow direction provided the observer is located at about the beaming angle  $\theta \approx 1/\gamma$ . At larger viewing angles this apparent emissivity asymmetry is reduced.

Filaments produced by the first elliptical body mode will reside within the jet and will dominate filaments produced by the surface elliptical wave mode whose apparent emissivity falls rapidly inside the jet surface. The helical first body mode (not shown) would generate a single bright twisted filament within the jet which would exhibit apparent emissivity asymmetry, similar to that illustrated in Figure 3 for the elliptical mode filaments, as the filament winds around the jet. The helical surface mode which twists the entire jet is found to result in little apparent emissivity variation [31].

## 6. Conclusion

Kelvin-Helmholtz instability induced normal mode pinch structures have been observed in axisymmetric non-relativistic and relativistic jet simulations, and normal mode helical, elliptical, triangular and rectangular structures have been observed in fully 3D non-relativistic jet simulations. In numerical simulations large amplitude helical and elliptical normal mode structures have been found to lead to significant mass entrainment. This mass entrainment slows “light” jets and prevents them from propagating to large distances while remaining highly collimated. The growth of large amplitude normal mode structures can be slowed by high magnetosonic Mach numbers. However, magnetic acceleration and collimation schemes produce jets which pass through a trans-Alfvénic and trans-magnetosonic region in which the growth rate of the normal modes can be very large. Numerical simulations show that “top hat” profile “light” non-relativistic jets will not survive this region. The helically twisted structures that we observe in numerical simulations are on much shorter spatial length scales than those of twisted structures seen at parsec and kiloparsec length scales on extragalactic jets.

If magnetic jet acceleration and collimation schemes are to prove viable for the production of observed jets that propagate to distances orders of magnitude larger than the location of the Alfvén point, they must flow through the transmagnetosonic region with sufficient stability. Additional stability both linearly and non-linearly may be achieved by different density, temperature, magnetic and velocity profiles, through rapid jet expansion [32] or by the embedding of a jet in a surrounding fast wind. In particular, a higher jet density relative to the surrounding environment will slow the development of instability. The high jet density of non-relativistic protostellar jets relative to the ambient and cocoon medium behind the jet bow shock should allow the jets to propagate with sufficient stability through a trans-Alfvénic region. For

galactic relativistic jets or extragalactic highly relativistic jets magnetic acceleration schemes would require that the Alfvén speed at the Alfvén point be near to or greater than lightspeed in order to produce a relativistic jet. In this case, theory indicates that relativistic effects can be stabilizing and lead to a scenario in which relativistic galactic and extragalactic jets can propagate through the trans-Alfvénic region with sufficient stability.

Once through the trans-Alfvénic region, continued jet expansion leads to supermagnetosonic flow. On the supermagnetosonic jet relativistic effects serve to reduce the distortion amplitude of normal mode structures, and this reduction in distortion amplitude should lead to a reduction in the mass entrainment that slows and disrupts jet collimation. Although distortion amplitudes are reduced the predicted pressure fluctuations combined with the Doppler boosting factor suggest that twisted filamentary structures should be readily visible on relativistic jets.

### Acknowledgements

This work was supported by the National Science Foundation through grants AST 9318397 and AST 9802955 to the University of Alabama and through grant AST 9617032 to the University of Michigan. Numerical work utilized the Pittsburgh Supercomputing Center and the Ohio Supercomputer Center.

### References

- [1] Levinson, A., & Blandford, R. 1996, *ApJ*, 456, L29
- [2] Cawthorne, T.V. 1991, in *Beams and Jets in Astrophysics*, ed. P.A. Hughes (Cambridge: CUP), 187
- [3] Mirabel, I.F., & Rodríguez, L.F. 1994, *Nature*, 371, 46
- [4] Hjellming, R.M., & Rupen, M.P. 1995, *Nature*, 375, 464
- [5] Tingay, S.J., et al. 1995, *Nature*, 374, 141
- [6] Zensus, J.A., Cohen, M.H., & Unwin, S.C. 1995, *ApJ*, 443, 35
- [7] Mirabel, I.F., & Rodríguez, L.F. 1995, *Annals of the New York Academy of Sciences*, eds. H. Böhringer, G.E. Morfill, & J. Trümper, 759, 21
- [8] Bicknell, G.V. 1994, *ApJ*, 422, 542
- [9] ———. 1995, *ApJS*, 101, 29
- [10] Meier, D.L., Payne, D.G., & Lind, K.R. 1996, in *IAU Symp. 175: Extragalactic Radio Sources*, eds. R. Eckers, C. Fanti & L. Padrielli, (Dordrecht: Kluwer), 433
- [11] Ouyed, R., Pudritz, R.E., & Stone, J.M. 1997, *Nature*, 385, 409
- [12] Ouyed, R., & Pudritz, R.E. 1997, *Nature*, 482, 712
- [13] Romanova, M.M., Ustyugova, G.V., Koldoba, A.V., Chechetkin, V.M., & Lovelace, R.V.E. 1997, *ApJ*, 482, 708
- [14] Meier, D.L., Edgington, S., Godon, P., Payne, D.G., & Lind, K.R. 1997, *Nature*, 388, 350
- [15] Camenzind, M. 1997, in *IAU Symp. 182: Herbig-Haro Flows and the Birth of Low Mass Stars*, eds. B. Reipurth & C. Bertout, (Dordrecht: Kluwer), 241
- [16] Livio, M. 1997, in *IAU Colloquium 163: Accretion Phenomena and Related Outflows*, eds. D.T. Wickramasinghe, G.V. Bicknell & L. Ferrario, (San Francisco: ASP), 845
- [17] Ray, T.P. 1981, *MNRAS*, 196, 195
- [18] Ferrari, A., Trussoni, E., & Zaninetti, L. 1981, *MNRAS*, 196, 1051
- [19] Fiedler, R., & Jones, T.W. 1984, *ApJ*, 283, 532
- [20] Bodo, G., Rosner, R., Ferrari, A., & Knoblock, E. 1989, *ApJ*, 341, 631
- [21] Appl, S., & Camenzind, M. 1992, *A&A*, 256, 354
- [22] Apple, S. 1996, in *ASP Conf. Series Vol. 100: Energy Transport in Radio Galaxies and Quasars*, eds. P.E. Hardee, A.H. Bridle & A.Zensus, (San Francisco: ASP), 129
- [23] Rosen, A., Hardee, P.E., Clarke, D.A., & Johnson, A. 1999, *ApJ*, 510, 136
- [24] Hardee, P.E., & Rosen, A. 1999, *ApJ*, in press
- [25] Birkinshaw, M. 1991, in *Beams and Jets in Astrophysics*, ed. P.A. Hughes (Cambridge: CUP), 278

- [26] Hardee, P.E., Clarke, D.A., & Rosen, A. 1997, *ApJ*, 485, 533
- [27] Hardee, P.E., Rosen, A., Hughes, P.A., & Duncan, G.C. 1998, *ApJ*, 500, 599
- [28] Hardee, P.E. 1983, *ApJ*, 269, 94
- [29] Hardee, P.E. 1999a, in preparation
- [30] Duncan, G.C. & Hughes, P.A. 1994, *ApJ*, 436, L119
- [31] Hardee, P.E. 1999b, in preparation
- [32] Hardee, P.E. 1987, *ApJ*, 313, 607